Proceedings of the ASME 2020 39th International Conference on Ocean, Offshore and Arctic Engineering OMAE 2020
June 28-July 3, 2020, Fort Lauderdale, FL, USA

OMAE2020-18830

TORQUE CONTROL OF A LABORATORY SCALE VARIABLE SPEED HYDROKINETIC TIDAL TURBINE - CFD SIMULATION AND VALIDATION

Arturo Ortega*
Institute for Energy Systems
The University of Edinburgh
Edinburgh, UK
arturo.ortega@ed.ac.uk

Anup Nambiar
Institute for Energy Systems
The University of Edinburgh
Edinburgh, UK
a.nambiar@ed.ac.uk

David Ingram
Institute for Energy Systems
The University of Edinburgh
Edinburgh, UK
david.ingram@ed.ac.uk

Danny Sale
Siemens Gamesa Renewable Energy
Boulder, USA
daniel.sale@siemensgamesa.com

ABSTRACT

Hydrokinetic tidal turbines are a promising alternative for the generation of clean electrical energy. They are still far behind, with respect to their technological development, in comparison to offshore wind turbines, which are currently in the stage of commercial energy production. Thus, more studies and analyses of the behaviour of tidal devices and their interaction with the surrounding ocean space are required. How this interaction is interrelated to the power production system is also necessary to be further examined. In this paper, the development of a whole system, fully-coupled model of a laboratory-scale hydrokinetic tidal turbine, along with its interactions with the ocean environment and its electrical control system is described. The model was developed in fastFlume (SOWFA, NREL) coupled with an external torque control system. The control system is developed from the optimal torque speed curve based Maximum Power Point Tracking (MPPT) algorithm. The optimal torque speed curve of the turbine used in the model was obtained from experimental work in a test tank. The hydrokinetic tidal turbine and the control system models were implemented independently. They were coupled in order to reach an energy balance between the surrounding flow, the tidal turbine, and the control system. Three flow stream velocities were imposed in the inlet of the model domain, starting the rotor from zero rotational speed. After the optimal rotational speed is attained, the electrical power generated and the loads experienced by the turbine rotor were studied. In the simulations, the tidal device is controlled to keep the optimal power production for any flow stream velocity. The results of the modelling work were compared with experimental measurements taken from 1:15th scaled testing of a fully-instrumented and controllable tidal device at the Flowave Ocean Energy Research Facility, The University of Edinburgh, a combined wave and current test facility. The results show time series of turbine and generator variables like mechanical and electrical torque and power, as well as thrust and the optimal rotational speed for each of the tested cases. The validation shows good agreement between the numerical and experimental results which encourages futures studies using the coupled model, including the turbine working in more complex flow conditions and controlled by more complex control schemes.

*Address all correspondence to this author.

Copyright © 2020 by ASME

INTRODUCTION

Small arrays of tidal turbines have been deployed in Europe over the last few years, but the technology is still not commercial yet. To become a commercially viable technology, the turbines will need to maintain high levels of reliability and will need to structurally withstand the large unsteady hydrodynamic loads introduced by the flow conditions. The behaviour of a hydrokinetic tidal turbine (HKT) interacting with the ocean environment as well as with it's electrical control system will need to be extensively studied. Such studies will give insights on improving turbine reliability and on identifying means to reduce turbine operation and maintenance costs.

The experience of operating a full-scale tidal turbine deployment gives us a full understanding of these characteristics, but is expensive. Tank testing of scaled models of turbines provides a cheaper alternative to understand better the interactions of the turbines with their environments and the power extraction process. CFD based numerical models of turbines provide a bridge between scaled-testing in tanks and full-scale deployments in actual tidal sites.

To accurately predict the turbine load and performance, the whole system - ocean environment - HKT - electrical control system, needs to be modelled and studied holistically. Numerous numerical modelling studies on HKTs have been published, but they have studied the ocean environment – HKT interaction or the HKT-control system interaction isolated from each other. A Generalised Actuator Disk CFD model (GAD-CFD) for horizontal wind and tidal turbines and their wakes was presented in [1]. The model considers correction of losses along the foil, foil cross section variation along the length, dynamic change of Reynolds number, and tip radius correction. The model also gives consideration to lift and drag coefficients' variation with thickness, surface roughness and Reynolds number. The model showed improvements compared to traditional previous models when validations against experimental results were carried out. A moving-domain CFD solver was designed in [2]. The solver was implemented by deploying the Arbitrary Lagrangian Eulerian Variational Multi-scale Formulation, working as a Large Eddy Simulation model, enhanced with weak enforcement of essential boundary conditions, acting as a wall model, into a open-source finite element automation software. The work showed good agreement against experimental measurements in terms of thrust and power for cases using uniform flow. A paper examining the HKT - control system interaction, exploring the effects of connecting supercapacitors at the DC link of a 1.5 MW three-bladed horizontal-axis tidal current turbine that uses a torque pulsation mitigation strategy is presented in [3]. The supercapacitor was shown to absorb the fast short-term variations of electrical power and keep the DC link voltage within limits. Results from that paper demonstrated that the DC link voltage and the grid side harmonics were positively influenced by the presence of the supercapacitor at the DC link.

This paper describes a CFD based, fully-coupled, numerical model of a laboratory scale HKT. The model follows the whole system approach mentioned earlier, and accurately simulates the ocean environment - HKT - electrical control system interactions. The electrical control system is modelled using a torque control based MPPT system founded on the turbine's optimal torque-speed curve. The numerical model is validated using measurements from tank testing of a scaled HKT model at the Flowave Ocean Research Facility, University of Edinburgh.

THE NUMERICAL MODEL

This section describes the whole system, time-domain, numerical model developed. The model consists of three independent subsystems, which are fully coupled with each other. The first subsystem is the ocean environment, which is simulated by CFD, the second is the HKT, which is simulated by Actuator Line Model (ALM), and the last one is the electrical control system. In this work reported, these three subsystem were coupled to work simultaneously in the time domain.

The Ocean Environment and HKT Models

In order to numerically model realistic operational conditions of a HKT inside a laboratory tank, the SOWFA simulator [4], developed by the National Renewable Energy Laboratory, was utilized. SOWFA is a simulator for wind turbines that helps users investigate wind turbine behaviour under different operating and environmental conditions. The turbine model of SOWFA was developed based on the Actuator Line Model (ALM) [5]. It is implemented entirely in C++ and is embedded into the OpenFOAM CFD toolbox [6]. Turbulence around the turbine is simulated by the OpenFOAM toolbox using the Large Eddie Simulation model (LES) [7]. SOWFA was implemented for wind turbines, however, the functionalities of SOWFA have been extended to allow the simulation of HKTs through the use of a particular model setup into SOWFA called fastFlume [8].

The flow around the turbine is highly turbulent and in order to capture this behaviour of the flow, LES has been used [9]. In LES, the larger turbulent scales are directly resolved by solving the spatially filtered Navier-Stokes equations, whereas the effects of the remaining, more isotropic, smaller scales are modelled with a subfilter-scale (SFS) turbulence model. The turbulence inflow generator is a custom boundary condition for the OpenFOAM toolbox. It calculates synthetic turbulence for the LES simulation. For this, the turbulence length scale, a reference velocity, and the Reynolds stresses need to be specified [10]. This turbulence inflow generator requires the turbulence length scale to be at least two times the mesh size. The fluctuating velocity components used for the calculation of the Reynolds stresses are approached as in Eqn.1:

Copyright © 2020 by ASME

$$u' = I \cdot u, \qquad v' = 0.75u', \qquad w' = 0.56u' \tag{1}$$

where I is the turbulence intensity, u is the magnitude of the reference velocity, and u', v' and w' are the fluctuating velocity components. The turbulence inflow generator produces turbulence time series that evolves inside the domain. The basic idea behind this method comes from the concept that turbulent flow is a motion of turbulence spots arising at random positions and at random times.

The model of the turbine rotor is based on the Actuator Line Model (ALM). The ALM discretizes the turbine blades as a sequence of equally spaced elements. In each blade element, drag and lift forces are calculated according to specified aerofoil data. In the ALM approach, the turbine blades react to the forces imposed by the environmental flow, applying body field forces by each blade element. From the point of view of the external ocean environment, the body forces can be considered as external perturbation forces against the ocean domain. The forces calculated by the ALM and applied to the environment are the body forces. They are considered in the Navier-Stokes equations as source terms. A body force is calculated for each blade element. These forces are projected to the control volumes using a Gaussian function shown in Eqn.2:

$$\vec{f_{turb}} = \frac{\vec{F}}{\varepsilon^3 \pi^{3/2}} e^{[-(r/\varepsilon)^2]} \tag{2}$$

where $\vec{f_{turb}}$ is the projected body force per unit volume, $\vec{F}$ is the force at the actuator element, ε defines the width of the projection, and r is the distance from the centre of the blade element to the centre of the control volume. The body force, which is imposed on the momentum equation, is equal and opposite to the lift and drag forces. By using the local velocity at the blade element, the lift and drag forces, and attack angle are calculated. The attack angle is considered to be the angle between the chord and the local flow velocity. Lift and drag coefficients are taking from tabulated airfoil data. The rotor power is calculated by multiplying the rotor torque, which is obtained by integrating the blade element torques across the length of the blade, times the rotor angular speed.

The Electrical Control System Model

The control system model used in this work is the optimal torque (OT) based Maximum Power Point Tracking algorithm [11]. The MPPT is a torque-control-based algorithm, which controls the tip speed ratio (TSR) of the HKT in order to achieve the highest possible power coefficient (C_P). Using the relationship between mechanical power and TSR, an expression for the HKT torque can be derived as a function of TSR and the angular rotor speed. By simplifying the torque expression further, the optimal HKT torque can be represented according to Eqn.3.

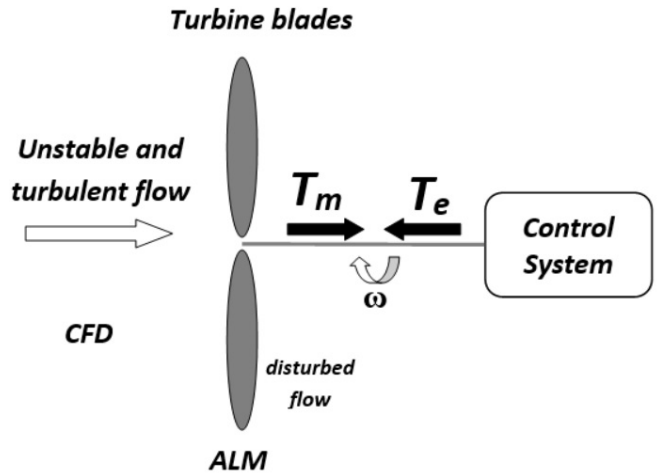

FIGURE 1. FULLY-COUPLED LES - ALM - CONTROL SYSTEM MODEL SCHEMATIC

$$T_{opt} = K_{opt}\omega^2 \tag{3}$$

In this expression, the constant K_{opt} is calculated by curve fitting of optimal torques versus angular speeds for a series of free tidal current speeds as discussed in Fig. 5. ω represents the rotor angular speed (rad/s). In this work, the constant K_{opt} for the turbine in question was obtained from experimental work which is further explained in the next section describing the experimental work.

The Fully-Coupled Whole System Model

Traditionally, HKTs and their control systems have been studied separately as monolithic systems, which, as discussed before, is one of the drawbacks of these models. Thus, one of the objectives of this work was to build a realistic, fully-coupled, model of an HKT – control system. As explained before, the ocean environment was simulated by LES/CFD and the HKT was modelled by the ALM approach. They are coupled with the control system, described in the previous section, by an energy balance relation between their mechanical and electrical torques, shown in Fig. 1.

The turbulent inflow from the inlet is disturbed by the body forces imposed by the HKT, which are calculated by the ALM approach. This means that the flow downstream of the HKT is highly disturbed. The hydrodynamic forces distributed along the

Copyright © 2020 by ASME

blades generate a resultant mechanical torque on the shaft, which connects the turbine rotor to the control system. The control system responds applying a resisting torque (electrical torque). This torque balance equation (Eqn. 4) results in the angular speed of the HKT being modified.

$$J\frac{d\omega}{dt} = T_e - T_m - B \cdot \omega \tag{4}$$

where T_e is the electrical torque (Nm), T_m is the mechanical torque (Nm), ω is the rotor angular speed (rad/s), J is the turbine and rotor inertia (kg-m^2), and B is the viscous friction (N-m-s/rad), which has been neglected in the simulations. In this work, the electrical torque is calculated using the equation for the optimal HKT torque as explained in the previous section.

The updated angular speed of the rotor will modify the turbulent/dynamic behaviour of the flow around the turbine blades. This in turn modifies the aerodynamic forces, the mechanical torque, the electrical torque and the angular rotor speed, and in turn the turbulent flow behaviour again. By incorporating this feature, the interactions of the full-coupled system is demonstrated.

EXPERIMENTAL SETUP AND METHODS

This section describes the experimental set-up and methods used to collect the experimental data that was used to validate the numerical model. This includes a brief description of the test facility used in this work, the turbines and their instrumentation, information on the flow and turbine load and performance measurements made.

Test Facility

All the experimental work reported in this paper was carried out at the Flowave Ocean Research facility (Flowave, https://www.flowave.eng.ed.ac.uk), located at the University of Edinburgh, UK [12]. Flowave is a circular, combined wave and current tank, with a diameter of 25 m and an operating water depth of 2 m (see Fig. 2). In the centre of the tank is a 15 m diameter, raisable, buoyant floor that provides access to the floor for model and instrumentation installation. Beneath the floor, along the entire tank circumference, are 28 impeller units that create a re-circulating flow system [13]. This arrangement of impellers allows the generation of a predominantly straight flow in any direction across the central test area of the tank [14]. The turbulence intensity is around 7% for the flow velocities used in these experiments. The tank can generate tidal current flow of up to 1.6 m/s. In the tests conducted, the turbine was exposed to current velocities of upto 1.0 m/s.

FIGURE 2. THE FLOWAVE OCEAN RESEARCH FACILITY

TABLE 1. GEOMETRICAL PARAMETERS OF THE MODEL HKT

Number of blades	3
Rotor diameter (m)	1.2
Hub diameter (m)	0.12
Hub location over tank bed (m)	1

Turbines and Instrumentation

The model scale turbine used in this work is a 1:15 scale, bed-mounted, fixed-pitch, three-bladed horizontal axis tidal turbine. It has a diameter of 1.2 m with the turbine rotor axis 1 m from the tank floor. The models were designed to be similar to the majority of full-scale prototypes [15, 16]. The model turbine, its blade geometry and installed instrumentation is described in detail in [17]. The blades were designed to provide a rotor thrust coefficient similar to a full-scale generic turbine across a wide range of tip speed ratios to provide full-scale similitude. Table 1 shows some of the geometrical parameters of the model turbine.

The turbine has an array of instrumentation, including sensors to measure the streamwise root bending moment for each blade RBM, torque Q and thrust T on the rotor. The generator in the turbine was simulated using a permanent magnet servo motor, directly connected to the rotor shaft. The motor provides a controllable resisting torque to the hydrodynamic torque imparted by the interaction of the flow and the turbine rotor. Rotor angular position θ was obtained from the motor encoder. The turbine was operated in speed control mode over a range of different tip speed ratios.

Flow Measurement

Ambient inflow measurements were made at rotor tip height, 2 diameters in front of the turbine, to characterise the inflow. These measurements were made using a Vectrino Profiler Acous-

Copyright © 2020 by ASME

tic Doppler Velocimeter (ADV) with a sampling rate of 100 Hz. At each measurement point/test, flow was measured for 300 s based on previous work at Flowave [18], after allowing the flow to reach steady state. The flow data was then quality checked and post-processed.

Table 2 summarises the specifications of all the turbine and additional instrumentation used in the tests.

Turbine Load and Performance Measurement

The experimental tests performed for this work included running TSR sweeps of the turbine at 5 different inflow current velocities – 0.6 m/s, 0.7 m/s, 0.8 m/s, 0.9 m/s and 1.0 m/s. From previous experiments with the turbine at Flowave, the power and thrust coefficients of the turbine were found to be Reynolds invariant above 0.6 m/s.

As mentioned earlier, the turbine was operated in speed control mode, wherein the turbine controller tries to keep the turbine's rotational speed at the user specified value. At each current velocity, the operating TSR of the turbine was modified by varying the rotational speed of the turbine. Load and performance data of the turbine, from the sensors and instrumentation discussed in the preceding section, were synchronously logged. Each test, at a particular current velocity and turbine speed, was performed for 300 s after having allowed the current velocity to reach steady state.

At 0.8 m/s current velocity, which is the design flow velocity of the turbine, the turbine was tested over TSRs from 3.5 to 13 with 0.5 increments. Fig. 3 shows the time series of load and performance parameters of the turbine operating at a TSR of 5.5 at this flow velocity. This TSR was found from previous testing to be the optimal TSR of the turbine.

At the other current velocities, only smaller number of TSR values around this optimum were tested. The power extracted by the turbine was obtained by multiplying the torque and angular speed measured. These measured load parameters and power were then averaged over the 300 s test duration. Fig. 4 shows plots of the average power extracted by the turbine versus the average turbine angular speed obtained from these tests at the five current velocities.

From the power-angular speed curves, the turbine angular speed corresponding to peak power extraction (around TSR 5.5) was determined for the current velocities tested. The turbine torque at these turbine angular speeds were obtained from the turbine torque-speed curves as shown in Fig. 5. The curve through these optimal torque versus speed points is the optimal torque speed curve of the turbine shown in Fig. 5. Through curve fitting, the optimal parameter K_{opt}, introduced in Eqn. 4, was determined for use in the numerical model runs. Table 3 shows the optimal torque, the maximum power extracted and thrust experienced by the turbine under the three current velocities. Table 4 shows the power, thrust and torque coefficients calculated for the

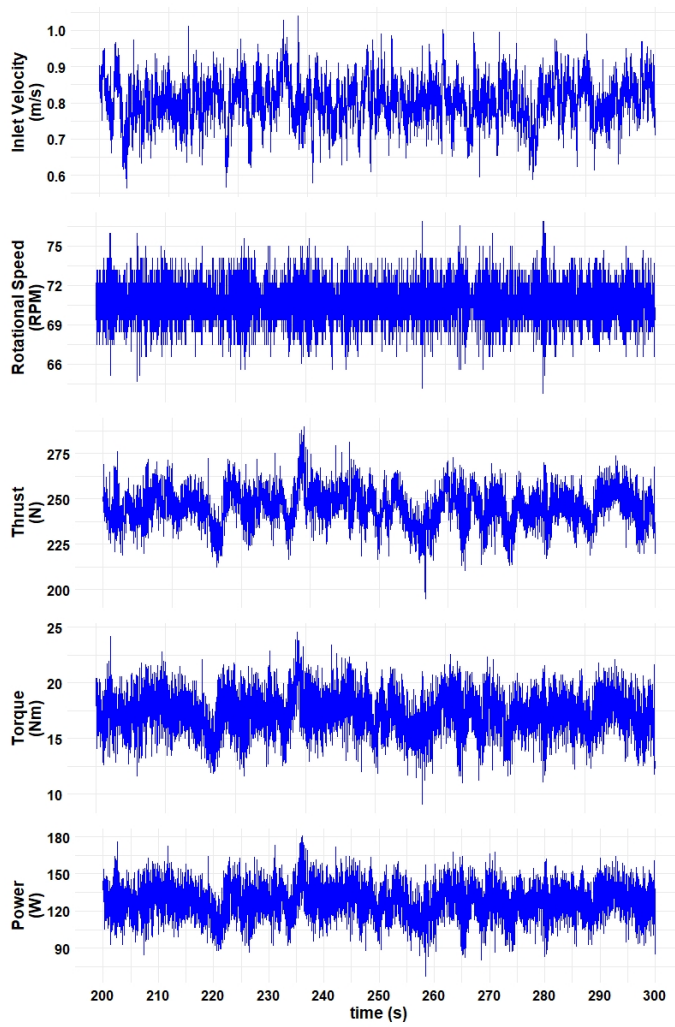

FIGURE 3. TIME SERIES OF CALIBRATED DATA MEASURED DURING FLOWAVE CAMPAIGN

optimal case at the three current velocities. The expressions used to calculate the performance coefficients are presented in Eqn.5.

$$C_T = \frac{T}{\frac{1}{2}\rho\pi R^2 U_o^2} \qquad C_Q = \frac{Q}{\frac{1}{2}\rho\pi R^3 U_o^2} \qquad C_P = C_Q \cdot TSR \quad (5)$$

where C_T, C_Q, and C_P are the thrust, torque, and power coefficients. T and Q are the thrust and torque values. ρ is the fluid density (1000 kg/m^3), R is the rotor radius, U_o is the free stream flow velocity, and TSR is the tip speed ratio.

The authors ran four series of tests with the turbine at Flowave over 2 years. At the start of every test phase, a set of benchmarking tests of the turbine in current were performed. The average load and performance data obtained from these bench-

Copyright © 2020 by ASME

TABLE 2. DESCRIPTION OF INSTALLED INSTRUMENTATION INCLUDING POSITION RELATIVE TO THE TURBINE ROTOR PLANE CENTRE

Type of instrumentation	Model	Variables measured	Sample Rate (Hz)	Location (m) X	Y	Z
ADV	Vectrino Profiler	U, V, W	100	-2.40	0	0.60
TST Instrumentation	UoE	T, Q, RBM, θ	256	0	0	0
Load Cell	AMTI OR6-7	F_X, F_Y, F_Z, M_X, M_Y, M_Z	256	0.49	0	-1.00

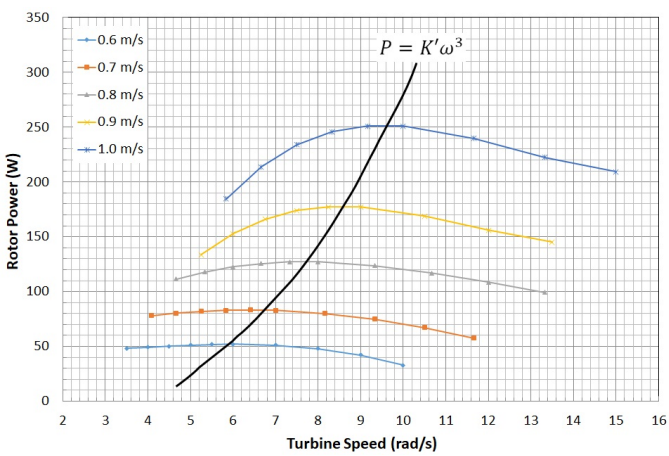

FIGURE 4. AVERAGE ROTOR POWER VERSUS AVERAGE ROTOR ANGULAR SPEED CHARACTERISTICS OF THE TURBINE FROM THE EXPERIMENTAL TESTS

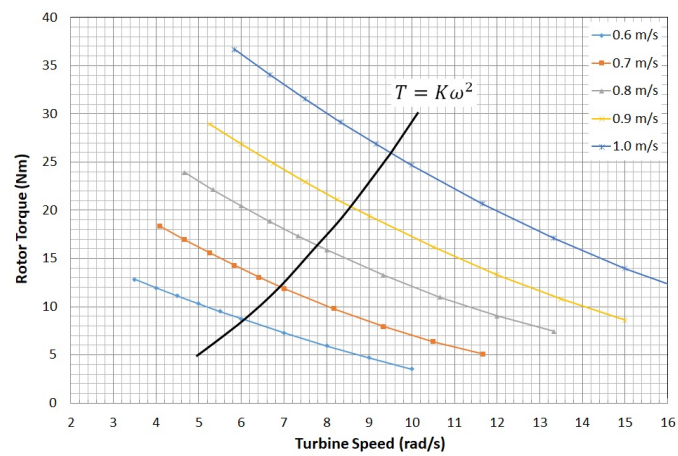

FIGURE 5. AVERAGE ROTOR TORQUE VERSUS AVERAGE ROTOR ANGULAR SPEED CHARACTERISTICS OF THE TURBINE FROM THE EXPERIMENTAL TESTS

marking tests, across the four phases, were extremely similar, which shows that the tests done were repeatable. The turbulence in the tank is not controllable, therefore, tests over 300 s were run to ensure that the standard deviation of the load and performance data were very similar across the four phases as well. Before every test phase, all the sensors used in the tests were calibrated, with sensor zeros taken multiple times during the day. These measures taken ensured the quality of the data obtained from the tests.

SIMULATION CASES SETUP

The domain, where the ALM model works, was set up as follows. The ocean environment was considered as a rectangular parallelepiped as shown in Fig. 6. At the inlet, a constant velocity profile was imposed together with the synthetic turbulence inflow generator [19]. At the outlet, the flow was considered to be fully developed. Therefore, a zero gradient boundary condition was imposed. The top, bottom and side borders were considered to be

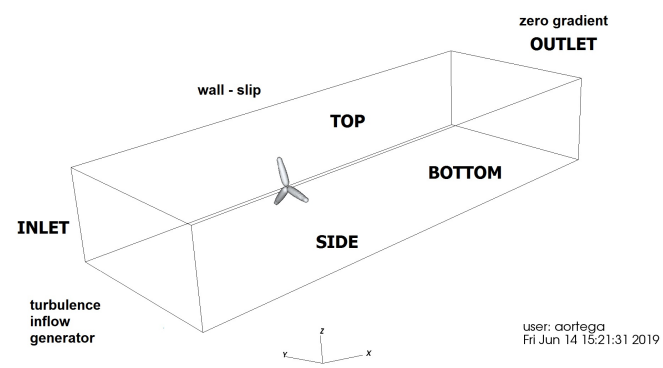

FIGURE 6. CFD DOMAIN FOR THE OCEAN ENVIRONMENT

symmetry borders. Therefore, a wall – slip boundary condition was applied in these borders.

The dimensions of the domain are as follows. In order to consider enough space for flow development, a length of 10.8 m

Copyright © 2020 by ASME

TABLE 3. AVERAGE TURBINE THRUST, TORQUE AND POWER AT THE OPTIMAL TORQUE POINT FROM THE EXPERIMENTAL TESTS

Uo (m/s)	Thrust (N)	Optimal Torque (Nm)	Maximum Power (W)
0.6	134.9022	9.5153	51.7841
0.7	183.9314	13.0613	83.3188
0.8	241.4914	17.3168	127.0294

TABLE 4. THRUST, TORQUE AND POWER COEFFICIENTS AT THE OPTIMAL TORQUE POINT FROM THE EXPERIMENTAL TESTS

Uo (m/s)	CT	CQ	CP
0.6	0.6627	0.0779	0.4285
0.7	0.6638	0.0786	0.4321
0.8	0.6673	0.0797	0.4386

downstream was considered. This length is nine-times the HKT diameter. The HKT was located three rotor diameters downstream of the inlet in order to allow the inlet synthetic turbulence to have enough domain to steady out. The remaining six rotor diameters to the outlet were arranged to avoid fluid-instability that can cause vortex breakdown. A water depth of 2 m was considered, which was the depth used in the experimental work at the Flowave facility. A transverse length of 4 m was considered to avoid the influence of lateral borders in the flow development, the high turbulence generated around the turbine, and the wake generated downstream of it. A uniform mesh distribution with a cell size equal to 0.018 m was considered. The total control volumes used in the CFD model were 600, 222, and 111 in x, y and z coordinates respectively.

The time step for the simulations was set according to the Courant-Friedrichs-Lewy condition (CFL). The blade tip velocity was used for the calculation of the CFL number. A reduction of the time step is necessary if the turbine rotational speed increases. In order to keep stability and accuracy, the blade tip was constrained to travel at most a control volume during each time step [7]. A Crank Nicolson scheme with a blending coefficient

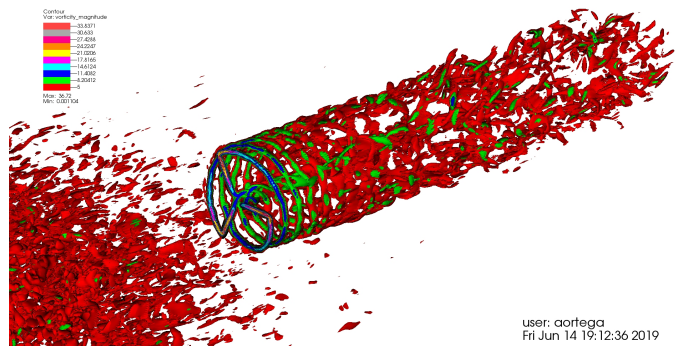

FIGURE 7. VORTICITY MAGNITUDE PREDICTED BY THE CFD SIMULATION

equal to 0.9 was used for the first order time derivate. Similarly, a Gauss linear scheme was selected for the gradients and divergences. For the turbulence, the Smagorinsky model was used for the LES modelling.

Blade elements were distributed uniformly along each blade according to the Blade Element Momentum Theory (BEMT) [20]. Forty blade elements per blade were used for the simulated HKT. The lift and drag coefficients used by the ALM are those presented in [21]. No additional three-dimensional corrections were considered in the simulations as LES is expected to capture these effects. The 1:15th scale HKT, described earlier in the paper, was modelled through the simulation. It's geometrical parameters were shown earlier in Table 1.

RESULTS AND ANALYSIS

The use of CFD allows detailed studies of the flow development in the domain and the analysis of the effects of the flow behaviour on the performance of the HKT. This section discusses the results of the simulations of the whole system model (ocean environment - HKT - electrical control system). Fig. 7 shows the wake development downstream of the HKT predicted by the simulations. Theoretically, the idea is to minimise the level of turbulence generated by the turbine rotor, and consequently increase the kinetic energy captured by the HKT. Fig. 8 shows a sample of the flow velocity magnitude at the rotor cross-section. The lowest speeds, shown by the blue colour in the figure, are located at the right-hand side of the blades as they rotate in the anticlockwise direction capturing kinetic energy.

The coupling of the CFD – ALM – control system in the model was validated using results from the experimental work with the HKT performed at the Flowave facility. Three constant velocities of 0.6 m/s, 0.7 m/s and 0.8 m/s at the inlet (see Fig. 6.) were imposed on the model. For the turbulence inflow generator, a turbulence intensity of 10% and a turbulence length scale equal to 0.108 m, which meets the criterion for the turbulence

Copyright © 2020 by ASME

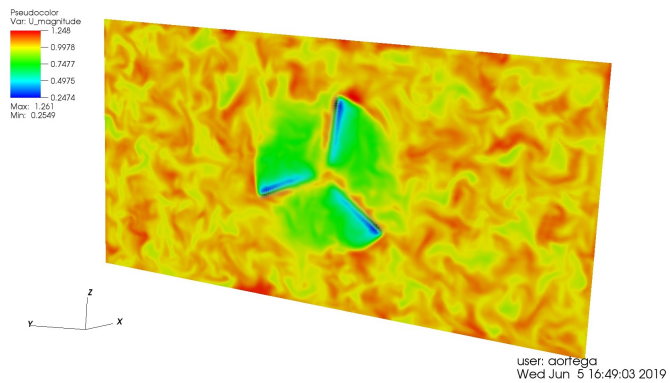

FIGURE 8. VELOCITY MAGNITUDE AT ROTOR CROSS-SECTION PREDICTED BY THE CFD SIMULATION

inflow generator, were considered. A time-step of 0.002 s was used in order to avoid numerical instabilities during the transient period. The inertia of the turbine-control system was assumed to be 1 kg-m^2 to test the performance of the coupling in the numerical model. This was accomplished by comparing the steady state values of the loads and performance parameters obtained from the numerical model with the experimental work. The first 20 s of the simulation allows the flow to develop over the tank. During this initial period, the turbine is at rest. The dynamic analysis of the HKT response to the control system starts at time equal to 20 s.

Fig. 9, Fig. 10 and Fig. 11 show the time-series of the turbine rotational speed, rotor thrust and rotor torque, at the three inflow current velocities obtained from the model. The transient periods in these time-series last for between four to five seconds according to the inflow current velocities. As the inflow current velocity increases, the rotational speed, the rotor thrust and torque are seen to increase as well. This is a feature of the fully-coupled model developed, which keeps the turbine operation at the optimal torque/TSR point at all times. In the case of rotor thrust, the increased inflow current velocity and the increased rotational speed of the turbine, which in turn causes a higher blockage, produces a higher thrust value when the flow velocity increases. Fig. 12 presents the time series of the rotor power for the three free stream flow velocities, which follow a similar profile as the parameters discussed above, since the rotor power is obtained by multiplying the rotor torque and the turbine angular speed.

Table 5 shows the average rotational speed, rotor thrust, torque and power, calculated for the stable period in the time-series, for the three current flow velocities. Fig. 13 shows the percentage errors in these values compared to the values presented in Table 3 from the experimental work. In the case of average rotor rotational speed the difference is negligible (a maximum of 0.75% at 0.8 m/s). The percentage errors in the average rotor thrust are the highest. They are between 6.78% and 8.77%

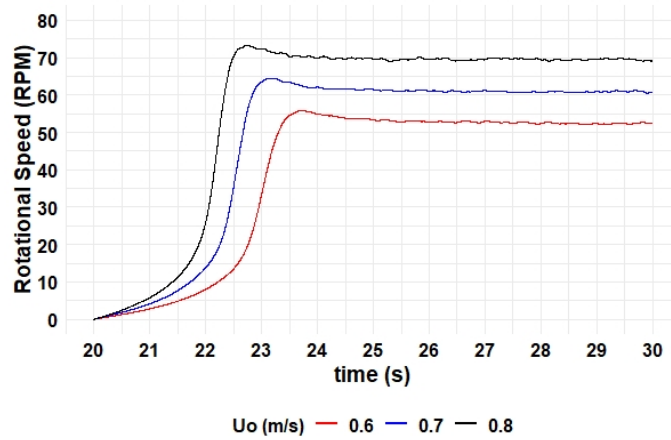

FIGURE 9. TIME-SERIES OF TURBINE ROTATIONAL SPEED FROM THE SIMULATION RUNS

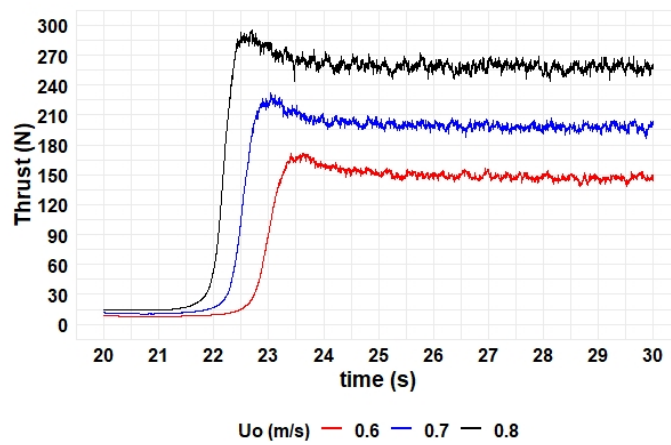

FIGURE 10. TIME-SERIES OF ROTOR THRUST FROM THE SIMULATION RUNS

for the three current velocities. It is suspected that these high errors in the average thrust are due to the fact that the turbine rotor model does not consider the thrust forces experienced by the turbine hub. The maximum percentage error between the simulated and measured average rotor torque is 3.13%. The maximum percentage error between the simulated and measured average rotor power is 3.89%, which is essentially the sum of percentage errors in the torque and speed. The simulation model developed gives a higher percentage error as the free stream velocity increases. This is true for the rotational speed, torque and power and can be explained by the turbulence around the rotor being more irregular and chaotic as the current velocity increases. The BEMT model is not able to capture the effects of increased turbulence, which explains this observation.

The power, torque and thrust coefficients from these simu-

Copyright © 2020 by ASME

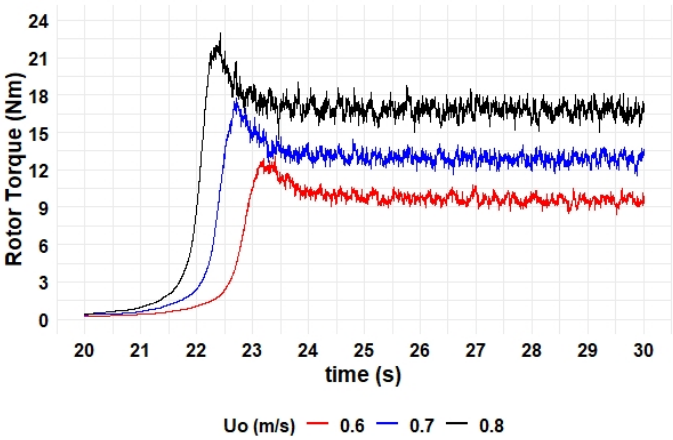

FIGURE 11. TIME-SERIES OF ROTOR TORQUE FROM THE SIMULATION RUNS

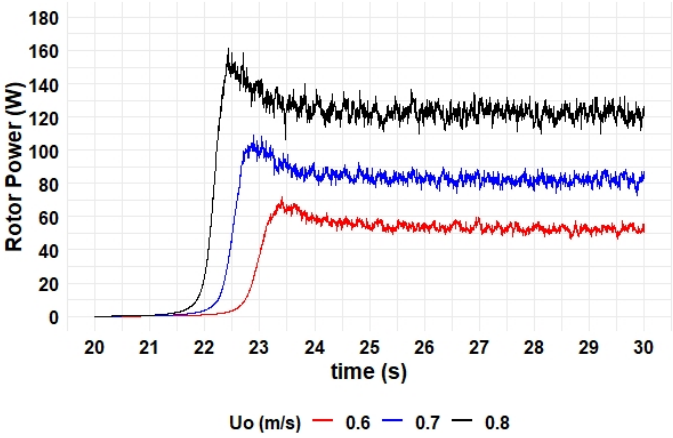

FIGURE 12. TIME-SERIES OF ROTOR POWER FROM THE SIMULATION RUNS

lation runs are presented in Table 6. They were calculated using the expressions presented in the Eqn. 5. Fig. 14 shows the percentage difference between the performance coefficients from the simulations and the experiments, which were shown in Table 4. As seen in the case of the absolute parameters, the highest percentage errors are seen for the thrust coefficient. The percentage errors in the torque and power coefficients increase with an increase in the free stream flow velocity. These characteristic were seen with the absolute average values of the parameters and have been explained earlier.

Finally, the time-series of the electrical torque and electrical power from the simulation runs are presented in Fig. 15 and Fig. 16 respectively. Their average values calculated during the stable period are presented in Table 7. Since an MPPT based controller was used in the numerical model, the mean values of

TABLE 5. AVERAGE TURBINE ROTATIONAL SPEED, THRUST, TORQUE AND POWER AT THE OPTIMAL TORQUE POINT FROM THE SIMULATION RUNS

Uo (m/s)	Rotational Speed (RPM)	Thrust (N)	Rotor Torque (Nm)	Rotor Power (W)
0.6	52.42	146.7324	9.5448	52.3941
0.7	60.86	197.9238	12.8758	82.0558
0.8	69.50	257.8626	16.7740	122.0868

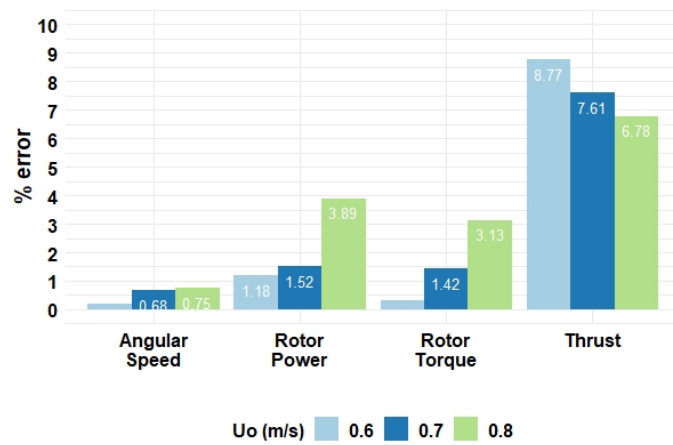

FIGURE 13. PERCENTAGE ERROR BETWEEN THE AVERAGES OF THE SIMULATED AND MEASURED QUANTITIES

the mechanical rotor torque and power are almost the same as the mean values of the electrical torque and power.

CONCLUSIONS

In this work, a numerical whole system model of a HKT, was presented and validated with experimental data. The model was used to analyse the loads experienced by and the performance of the HKT under realistic flow and turbulence conditions. The novel feature of the HKT model is that it is fully-coupled with its control system as well as with the ocean environment. The ocean environment was simulated using a CFD model, which was comprised of an LES turbulence model and a synthetic turbulence inflow generator. The ALM approach was used to model the turbine rotor. The interactions between the surrounding ocean environment and the HKT were incorporated by the generation of body forces to the environment, which is the response of the ap-

Copyright © 2020 by ASME

TABLE 6. THRUST, TORQUE AND POWER COEFFICIENTS AT THE OPTIMAL TORQUE POINT FROM THE SIMULATION RUNS

Uo (m/s)	CT	CQ	CP
0.6	0.7108	0.0771	0.4230
0.7	0.7044	0.0764	0.4172
0.8	0.7027	0.0762	0.4159

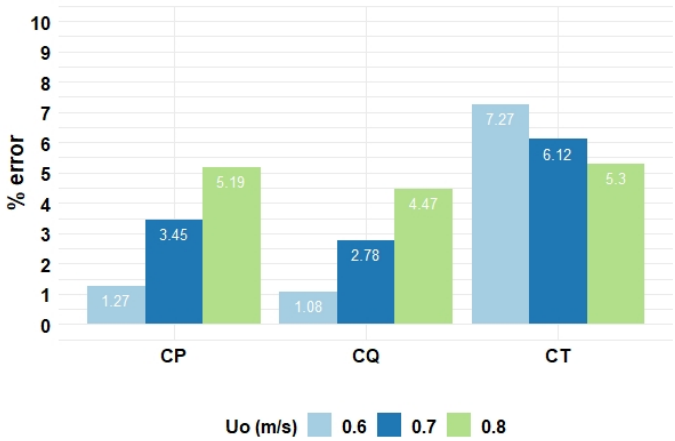

FIGURE 14. PERCENTAGE ERROR BETWEEN PERFORMANCE COEFFICIENTS FROM THE SIMULATIONS AND THE EXPERIMENTS

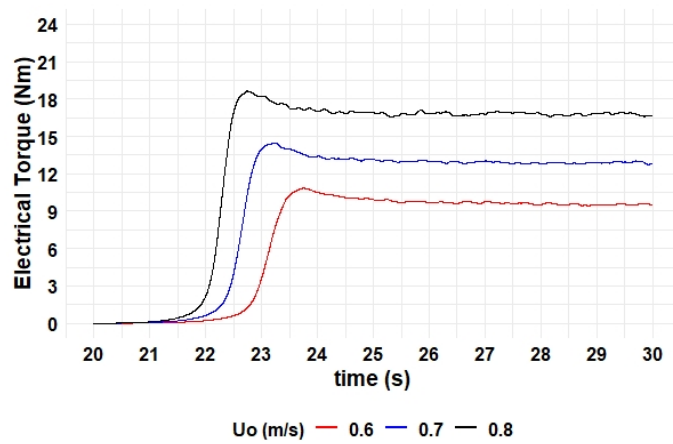

FIGURE 15. TIME SERIES OF ELECTRICAL TORQUE FROM THE SIMULATION RUNS

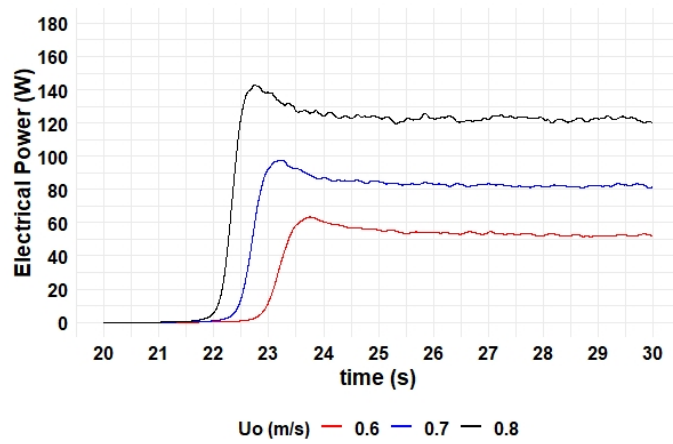

FIGURE 16. TIME SERIES OF ELECTRICAL POWER FROM THE SIMULATION RUNS

plied hydrodynamic forces on the turbine rotor. The interactions of the HKT and its control system were based on the torque energy balance relationship. The experimental data used to validate the fully-coupled, whole system, numerical model was obtained from experimental tests with a 1:15th scale tidal turbine model performed at the Flowave Ocean Research Facility.

The time-series of the turbine rotational speed, rotor thrust, torque and power presented in the paper, from simulation runs of the fully-coupled numerical model, showed the characteristics of the flow. The optimal rotational speed and torque at the three different current velocities tested were successfully achieved and maintained by the control system of the numerical model. The percentage difference between the average values of the thrust, mechanical torque and power were found to be low when comparing the numerical model results with the experimental data. This gives confidence on the model and allows its use for further studies.

At higher current velocities, the percentage errors between the simulated and measured quantities increased. This is attributed to the increased turbulence at higher flow velocities and the fact that the ALM based model does not consider turbulence effects. The model will be tested further under higher current velocities and developed further to improve its performance.

Finally, the possibility of adding a full electrical system, including the generator and the electrical network, in the control system used in this work will be pursued. The development of such a model will allow studies of the bi-directional impacts of the turbine on the electrical network and of the electrical network on the HKT.

Copyright © 2020 by ASME

TABLE 7. AVERAGE ELECTRICAL TORQUE AND ELECTRICAL POWER AT THE OPTIMAL TORQUE POINT FROM THE SIMULATION RUNS

Uo (m/s)	Electrical Torque (Nm)	Electrical Power (W)
0.6	9.5522	52.4365
0.7	12.8743	82.0464
0.8	16.7944	122.2422

ACKNOWLEDGMENT

This work was fund by the European Commission H2020 Programme for Research & Innovation - "Advanced monitoring, simulation and control of tidal devices in unsteady, highly turbulent realistic tide environments (RealTide Project)", Grant Agreement No 727689.

REFERENCES

[1] Edmunds, M., Williams, A., Masters, I., Banerjee, A., and VanZwieten, J., 2020. "A spatially nonlinear generalised actuator disk model for the simulation of horizontal axis wind and tidal turbines". *Energy The International Journal,* ***194***, pp. 1–13.

[2] Zhu, Q., and Yan, J., 2019. "A moving-domain CFD solver in FEniCS with applications to tidal turbine simulations in turbulent flows". *Computers and Mathematics with Applications*.

[3] Sousounis, M., Shek, J., and Sellar, B., 2019. "The effect of supercapacitors in a tidal current conversion system using a torque pulsation mitigation strategy". *Journal of Energy Storage,* ***21***, pp. 445–459.

[4] Churchfield, M. and Lee, S., 2012. Simulator for Wind Farm Applications - SOWFA. https://nwtc.nrel.gov/SOWFA. Retrieved: January 2020.

[5] Sorensen, J., and Shen, W., 2002. "Numerical modeling of wind turbine wakes". *J. Fluids Eng,* ***124***, pp. 393–399.

[6] OpenCFD Ltd. The OpenFOAM Foundation. https://openfoam.org/. Retrieved: January 2020.

[7] Martinez, L.A. and Leonardi, S., 2013. Wind Turbine Modelling for Computational Fluid Dynamics. Tech. Rep. NREL/SR-5000-55054.

[8] Sale, D., and Aliseda, A., 2016. "The flow field of a two-blades horizontal axis turbine via comparison of RANS and LES simulations against experimental PIV flume measurements". In Proceedings of the 4th Marine Energy Technology.

[9] Churchfield, M., Li, Y., and Moriarty, P., 2013. "A large-eddy simulation study of wake propagation and power production in an array of tidal-current turbines". *Philosophical Transactions of the Royal Society A,* ***371***, pp. 1–15.

[10] Institute for Modeling and Numerical Simulation at the University of Rostock, 2015. https://github.com/LEMOS-Rostock/LEMOS-2.4.x. Retrieved: January 2020.

[11] Kumar, D., and Chatterjee, K., 2016. "A review of conventional and advanced MPPT algorithms for wind energy systems". *Renewable and Sustainable Energy Reviews,* ***55***, pp. 957–970.

[12] Ingram, D., Wallace, R., Robinson, A., and Bryden, I., 2014. "The design and commissioning of the first, circular, combined current and wave test basin". In Proceedigns of the OCEANS 2014, pp. 1–7.

[13] Robinson, A., Ingram, D., Bryden, I., and Bruce, T., 2015. "The generation of 3D flows in a combined current and wave tank". *Ocean Engineering,* ***93***, pp. 1–10.

[14] Noble, D. R., Davey, T., Smith, H. C. M., Kaklis, P., Robinson, A., and Bruce, T., 2015. "Characterisation of spatial variation in currents generated in the FloWave Ocean Energy Research Facility". In Proceedings of the 11th European Wave and Tidal Energy Conference, pp. 1–8.

[15] Parkinson, S. G., and Collier, W. J., 2016. "Model validation of hydrodynamic loads and performance of a full-scale tidal turbine using Tidal Bladed". *International Journal of Marine Energy,* ***16***, pp. 279–297.

[16] MeyGen Ltd., 2016. MeyGen Tidal Energy Project Phase 1. Project Environmental Monitoring Programme, Technical Report. Tech. Rep. MEY-1A-70-HSE-018-I-PEMP.

[17] Payne, G. S., Stallard, T., and Martinez, R., 2017. "Design and manufacture of a bed supported tidal turbine model for blade and shaft load measurement in turbulent flow and waves". *Renewable Energy,* ***107***, pp. 312–326.

[18] Sutherland, D. R. J., Noble, D. R., Steynor, J., Davey, T. A. D., and Bruce, T., 2017. "Characterisation of Current and Turbulence in the FloWave Ocean Energy Research Facility". *Ocean Engineering,* ***139***(May), pp. 103–115.

[19] Kornev, N., and Hassel, E., 2007. "Method of random spots for generation of synthetic inhomogeneous turbulent field with prescribed autocorrelation functions". *Communications in Numerical Methods in Engineering,* ***23***, pp. 35–43.

[20] Manwell, J.and Macgowan, J., and Rogers, A., 2009. *Wind Energy Explained – Theory, Design and Application*. Wiley.

[21] Bahaj, A., Batten, W., and McCann, G., 2007. "Experimental verifications of numerical predictions for the hydrodynamic performance of horizontal axis marine current turbines". *Renewable Energy,* ***32***(15), pp. 2479–2490.

Copyright © 2020 by ASME